ACS APPLIED MATERIALS & INTERFACES

Research Article

www.acsami.org

Supercapacitor Studies on NiO Nanoflakes Synthesized Through a Microwave Route

Subbukalai Vijayakumar, Sadayappan Nagamuthu, and Gopalan Muralidharan*

Department of Physics, Gandhigram Rural Institute—Deemed University, Gandhigram, Tamilnadu, India

Supporting Information

ABSTRACT: NiO nanomaterial was synthesized at different calcination temperatures using cetyltrimethyl ammonium bromide (CTAB) as surfactant via microwave method. Thermogravimetric studies revealed the decomposition details of $Ni(OH)_2$ precursor. The structure and morphology of the NiO was characterized by X-ray diffraction (XRD), Fourier transform infrared spectroscopy (FTIR), scanning electron microscopy (SEM), and transmission electron microscopy (TEM). NiO calcined at 300 °C shows a nanoflake-like structure. A possible formation mechanism has been discussed with time evolution study. Electrochemical studies indicate that the sample calcined at 300 °C exhibits better charge storage. The NiO nanoflakes exhibit maximum specific capacitance of 401 F g^{-1} at a current density of 0.5 mA cm^{-2}. The energy generated and hence the charges collected from wind and solar panels are slow but in many applications the power delivery has to be at a faster rate. Considering this aspect, slow-charge and fast-discharge tests have been performed and reported. The NiO nanoflakes appear to be a promising electrode material for supercapacitor application.

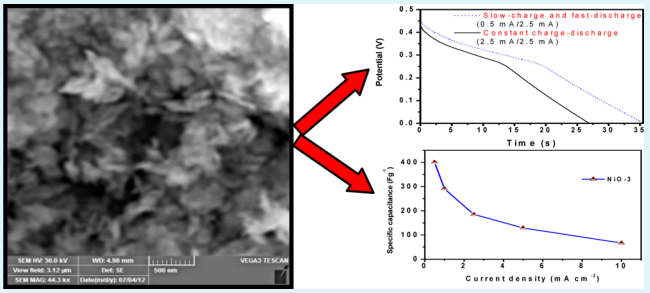

KEYWORDS: *microwave synthesis, nickel oxide, nanoflakes, supercapacitor, slow-charge and fast-discharge, impedance*

1. INTRODUCTION

In electrical energy storage, electrochemical supercapacitors receive increasing attention due to the features of delivering higher power than batteries and higher energy density than conventional capacitors. In addition, supercapacitors have some advantages over batteries, ie., longer cycle life, safer, no memory effect, and requirement of a simple charging circuit.[1,2] Supercapacitors can be used in hybrid electric vehicles with batteries or fuel cells to provide higher power during acceleration and to recover the energy during braking.[3] Supercapacitors can be classified by their charge storage mechanism into two categories. The first is electric double layer capacitors (EDLC), and the second is pseudocapacitors. EDLCs store charges using reversible adsorption of ions at the electrode and electrolyte interface while pseudocapacitors store charges by redox reactions on the surface of the electrode.[4] The low energy density of EDLCs has limited their applications. Ruthenium oxide has been extensively studied as a pseudocapacitor electrode material due to its high specific capacitance in acidic electrolyte.[5] However, the expensive and toxic nature of ruthenium oxide limits its commercialization. In this context, various metal oxides such as MnO_2, NiO, Co_3O_4, MoO_3, and TiN have been studied as possible candidates for supercapacitor applications.[6−10]

NiO is one of the materials suitable for pseudocapacitor electrode applications owing to its high theoretical specific capacitance, low cost, and high chemical and thermal stability.[11] The electrochemical performance of NiO nanostructures is strongly influenced by its morphology. NiO as an electrode material for supercapacitors, in the form of nanoflakes,[12] nano/microspheres,[13] quasi-nanotubes,[14] and nanosheet hollow spheres,[15] has been reported. Among these, nanoflakes have several advantages in supercapacitor applications. The nanoflakes enhance the diffusion of electrolyte and provide more paths for diffusion of ions leading to improvement in the performance of the electrode material.[16]

The NiO nanoflakes can be synthesized by various methods such as precipitation[12] and hydrothermal method,[17] but microwave assisted heating is an easy route of obtaining these morphologies. Microwave heating increases the reaction kinetics that induce the quick formation of nanoflakes by oriented attachment.[18] Generally, microwave assisted synthesis has many advantages, such as fast synthesis, increased phase purity, uniform particle size distribution, and morphology control.[19] Microwave assisted synthesis not only reduces the reaction time but also suppresses side reactions and thus improves the reproducibility.[20] Microwave chemistry is based on effective heating of material rather than inducing chemical reactions of electromagnetic radiation. This heating mechanism includes dipolar polarization and ionic conduction.[20] Obermayer et al.[21] confirmed the enhancement of growth kinetics in microwave assisted synthesis to be purely due to temperature

Received: January 2, 2013
Accepted: March 4, 2013
Published: March 4, 2013

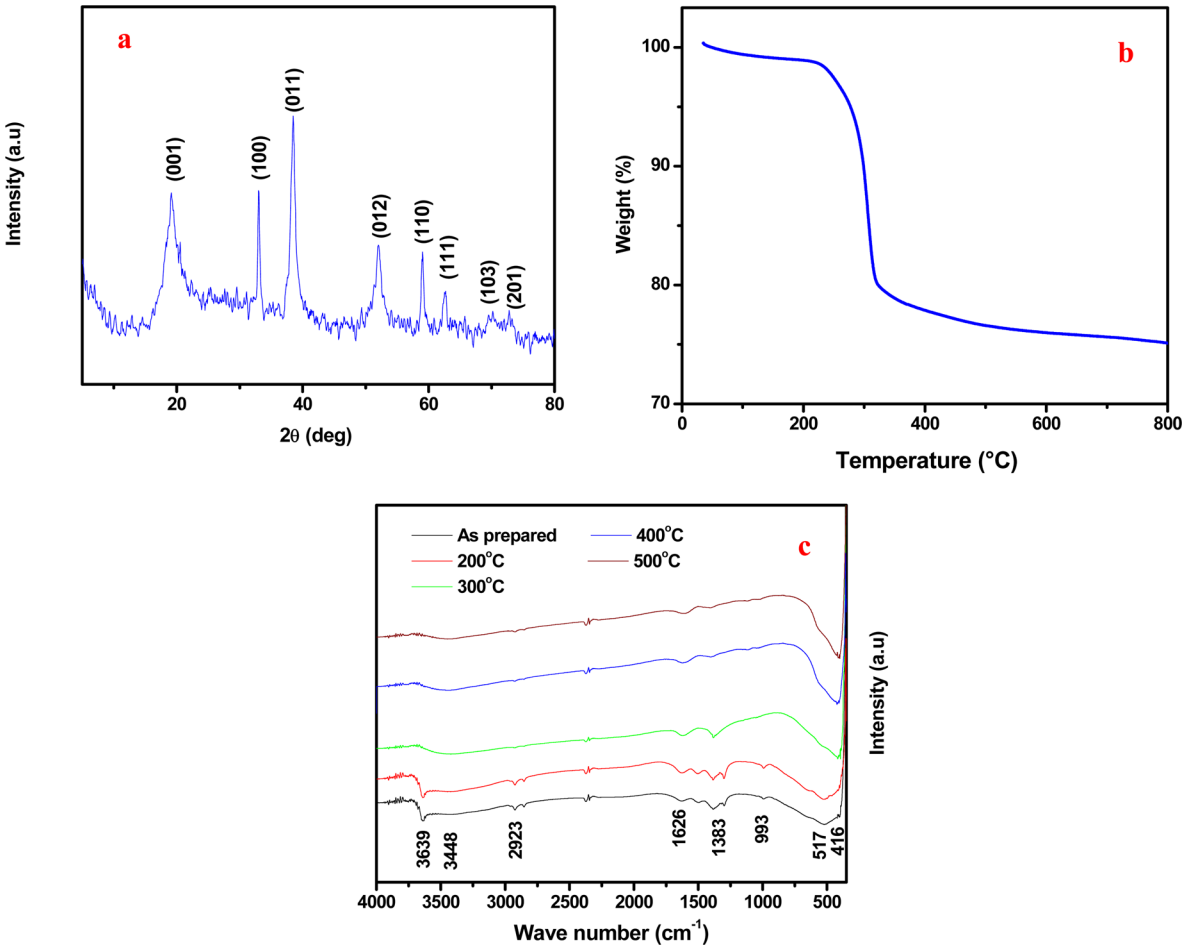

Figure 1. (a) XRD pattern of the as prepared samples, β-$(NiOH)_2$, before calcination, (b) TGA of uncalcined sample, and (c) FTIR spectra of as prepared samples and samples calcined at different temperatures.

effect and not due to the influence of electromagnetic reaction. There are numerous reports on the synthesis of NiO with different nanostructured configurations and morphologies via microwave method for possible use in supercapacitor applications. For example, NiO nanoflowers synthesized by microwave method at 15 min of microwave heating exhibit maximum specific capacitance of 277 F g^{-1} at scan rate of 2.5 mV s^{-1}.[22] Cao et al.[23] reported maximum specific capacitance of 770 F g^{-1} at discharge current of 2 A g^{-1} for flowerlike NiO hollow nanosphere synthesized using the gas/liquid interface via a microwave method at 170 °C in 3 min of microwave treatment and heat treatment of particles at 170 °C for 30 min. Meher et al.[24] reported the synthesis of porous ball like NiO by nonhydrothermal microwave-reflux at 120 °C for 15 min. It was reported to exhibit maximum specific capacitance of 420 F g^{-1} at 0.5 A g^{-1}.

In this paper, we report a 5 min synthesis of NiO nanoflakes using the microwave method using cetyltrimethyl ammonium bromide (CTAB) as a surfactant. Time evolution study has been performed, and a possible mechanism of formation of nanoflake structured NiO has been proposed in a pictorial manner. The electrochemical performance of NiO nanostructures, prepared via a microwave-assisted method and calcination at 300, 400, and 500 °C, as a supercapacitor electrode material in 2.0 M KOH electrolyte, has been reported and discussed.

2. EXPERIMENTAL METHOD

2.1. Material Synthesis. Nickel oxide nanoflakes were synthesized by a microwave-assisted method. In a typical synthesis, 25 mL of 40 mM of nickel nitrate hexahydrate ($(Ni(NO_3)_2{\cdot}6H_2O)$) was added to 25 mL of 20 mM of cetyltrimethyl ammonium bromide (CTAB), with continuous stirring. Then, the pH of the solution was increased to 10 by drop by drop addition of ammonia. The resultant solution was transferred into an autoclavable Pyrex glass bottle and closed with a polypropylene screw cap. The solution inside the pyrex glass bottle was subjected to 240 W of microwave radiation for 5 min using a household microwave oven (ONIDA). After cooling, the precipitate was collected by centrifugation. Then, the precipitate was dried overnight in an atmosphere of air at 60 °C. Finally the as prepared nanoparticles are converted into NiO nanopowder by calcining at 300, 400, and 500 °C for 1 h in an atmosphere of air. The samples prepared under various calcining temperatures are denoted as NiO-3, NiO-4, and NiO-5. For example NiO-3 denotes the NiO nanoflakes calcined at 300 °C.

2.2. Material Characterization. Thermogravimetric analysis (TGA) of the sample was performed using EXSTAR6200 TGA from SII Nanotechnology Inc., Japan, at a heating rate of 20 °C min^{-1} from room temperature to 800 °C. Perkin-Elmer SPECTRUM BX II spectrometer was employed to record the FTIR spectra. The X-ray diffraction (XRD) measurements were made with the help of Panalytical XPERT−PRO X-ray diffractometer with Cu Kα (1.5406 Å) radiation. The grain size of the NiO samples was estimated using Debye−Scherrer equation. The surface morphology of the NiO nanoflakes was studied by means of scanning electron microscope (SEM), Tescan VEGA-3 LMU Instrument. Hitachi H-7100 KVA was used to obtain the TEM images.

2.3. Electrode Preparation and Electrochemical Measurements. The active material NiO, activated carbon, and polytetrafluoro-ethylene were mixed in the ratio 80:15:5 using mortar and pestle with addition of ethanol. The slurry was coated on to a graphite sheet of area 1 cm^2. A 0.8 mg portion of active material was used as the loading material. The electrochemical performance was analyzed using CHI 660 D Electrochemical workstation. The electrochemical measurements were carried out using three electrode cell configuration with NiO as the working electrode, platinum as the counter electrode, and Ag/AgCl as the reference electrode with 2.0 M KOH as the electrolyte. The cyclic voltammetry measurements of the NiO electrode was performed at different scan rates in a potential window of 0 to 0.45 V. The charge−discharge characterization was performed at different current densities within a potential window of 0−0.45 V. Electrochemical impedance measurements were carried out between 0.01 Hz and 100 kHz with AC amplitude of 5 mV and bias potential of 0.4 V.

3. RESULTS AND DISCUSSION

3.1. Thermogravimetric and Structural Studies. The XRD pattern of as prepared (uncalcined) sample is shown in Figure 1a. The diffraction peaks at 19.2°, 32.98°, 38°, 52°, 58.98°, 62.55°, 70.2°, and 72.74° correspond to the (001), (100), (011), (012), (110), (111), (103), and (201) planes of hexagonal β-$Ni(OH)_2$ (JCPDS 74-2075). The absence of any other peaks confirms the phase purity of the $Ni(OH)_2$. Thermogravimetric studies were carried out to understand the phase changes and decomposition details of the as prepared β-$Ni(OH)_2$ sample. Figure 1b shows the TGA curve of the β−$Ni(OH)_2$ sample. A three-step weight loss, room temperature (RT)−200, 250−350, and 350−800 °C has been observed from the TGA curve. The sharp weight loss around 290 °C is an indication of complete conversion of $Ni(OH)_2$ to NiO. In addition, to identify and understand the behavior of $Ni(OH)_2$ on heat treatment (calcination), FTIR spectra have been recorded for as prepared samples and samples calcined in air at 200, 300, 400, and 500 °C. The spectra are shown in Figure 1c. As prepared and samples calcined at 200 °C reveal a band centered at 3639 cm^{-1} attributable to the stretching vibrational mode of non-hydrogen-bonded, free hydroxyl groups.[25] The broad band at 3448 cm^{-1} that could be observed in all the samples is due to the hydrogen-bonded hydroxyl groups.[25] The band at 1626 cm^{-1} corresponds to bending mode of interlayer water.[25] The peaks at 1383 and 993 cm^{-1} are due to the interlayer NO_3^- molecule.[18] A band centered at 517 cm^{-1} observed only with as-prepared samples and samples calcined at 200 °C corresponds to the vibration of δ O−H of hydroxyl group.[26] The absence of this band in the FTIR spectra of samples calcined above 200 °C indicates the removal of water. The band at 416 cm^{-1} corresponds to stretching vibration of NiO.[25] Thus, we conclude that the first minor weight loss that occurs between RT and 200 °C corresponds to the removal of adsorbed water. The second weight loss of ∼18% occurs between 250 and 350 °C and corresponds to the conversion of $Ni(OH)_2$ to NiO. If we consider conversion of $Ni(OH)_2$ to NiO, a weight loss of about 20% is to be expected. The weight loss as measured in the present work agrees with these expectations to a large extent.[24] The FTIR spectra of samples calcined at 200 and 300 °C confirm the transformation of $Ni(OH)_2$ to NiO at 300 °C. This could explain the second weight loss. The third weight loss between 350 and 800 °C is small. Figure 2 shows the XRD pattern of samples NiO-3, NiO-4, and NiO-5. All the diffraction peaks are indexed to the cubic phase of NiO. The peaks at 37.2°, 43.2°, 62.8°, 75.3°, and 79.4°

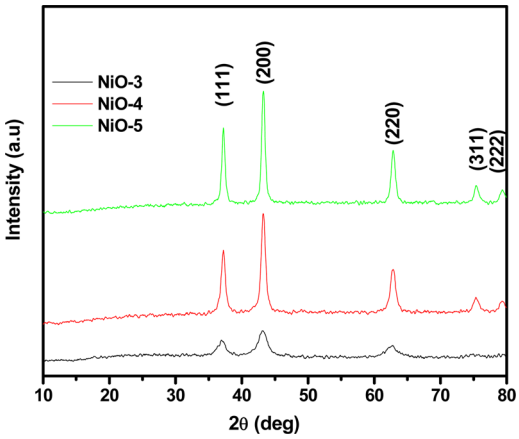

Figure 2. XRD pattern after calcination at different temperatures.

correspond to the (111), (200), (220), (311), and (222) planes of nickel oxide (JCPDS 78-0429). The degree of crystalinity increases while increasing calcination temperature. The average grain size as estimated from the XRD using Debye−Scherrer formula for the (111), (200), and (220) planes of the NiO is 6, 13, and 15 nm, respectively, for NiO-3, NiO-4, and NiO-5.

3.2. Morphological Study and Possible Formation Mechanism. The morphology of the β-$Ni(OH)_2$ sample and NiO samples are characterized using SEM. Figure 3 shows the SEM images of β-$Ni(OH)_2$ sample synthesized at 5 min of microwave treatment (without calcination) at different magnifications. SEM images clearly reveal a flakelike structure of the $Ni(OH)_2$. Figure 4a−c shows the SEM image of NiO-3, NiO-4, and NiO-5, and Figure 4d shows the TEM image of NiO-3. The SEM image of NiO-3 shows the nanoflakelike structure. It is worth mentioning that the SEM image of NiO calcined at 300 °C shows almost a similar morphology to that of $Ni(OH)_2$. The TEM image of NiO-3 reveals the nanoflake structure. A close observation of the TEM image indicates that the flakes are composed of nanoparticles. Xu et al.[18] reported the flakes to be composed of nanoparticles. The SEM image of NiO-4 reveals the aggregated flakelike structure which NiO-5 shows as an aggregated structure. In general, increase of the calcination temperature leads to aggregation and loss of specific morphology.[27] Since the reaction kinetics of microwave heating is very fast, it is ease to obtain the flakelike morphology within a short duration of the reaction. In order to understand the possible growth mechanism of NiO nanoflakes, microwave irradiation of precursor was carried out for different durations of exposure. Figure 5a−e shows the $Ni(OH)_2$ synthesized from 1 to 5 min by microwave heating. Before any microwave treatment, the precursor was bluish in color. After 1 min of microwave treatment, the solution color remains same (blue). The SEM image of $Ni(OH)_2$ treated for 1 min does not show any specific morphology which may be due to incomplete reaction. The solution treated for 2 min appears greenish in color. The SEM image of $Ni(OH)_2$ treated for 2 min indicates the formation of nanoparticles. The SEM image of $Ni(OH)_2$ treated for 3 min shows the rodlike structure due to aggregation of nanoparticles. SEM images of $Ni(OH)_2$ treated for 4 and 5 min shows a nanoflakelike structure. After 5 min of microwave heating, β-$Ni(OH)_2$ nanoflakes are formed due to oriented attachment. We have made an attempt to explain the formation of the nanoflakelike morphology in a pictorial manner. Scheme 1 shows the plausible mechanism for the formation of NiO

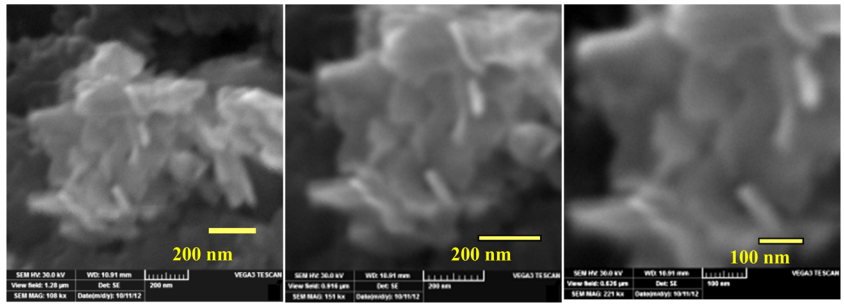

Figure 3. SEM images of as prepared sample (without any calcination).

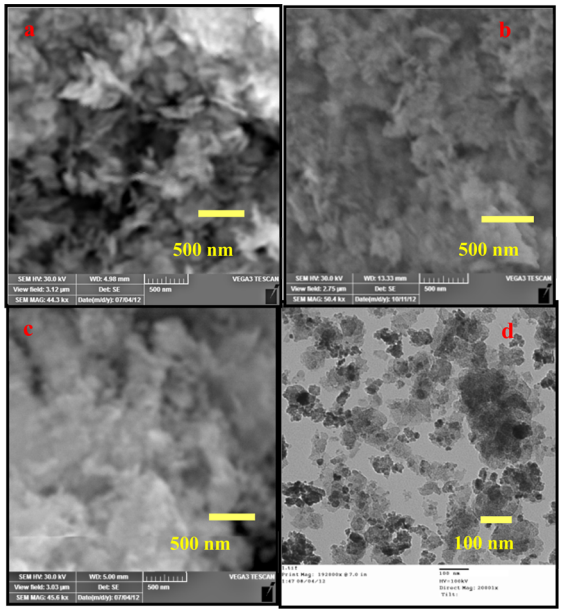

Figure 4. SEM images of sample calcined at (a) 300, (b) 400, and (c) 500 °C and (d) TEM image of sample calcined at 300 °C.

Scheme 1. Pictorial Representation of the Mechanism for the Formation of NiO Nanoflakes

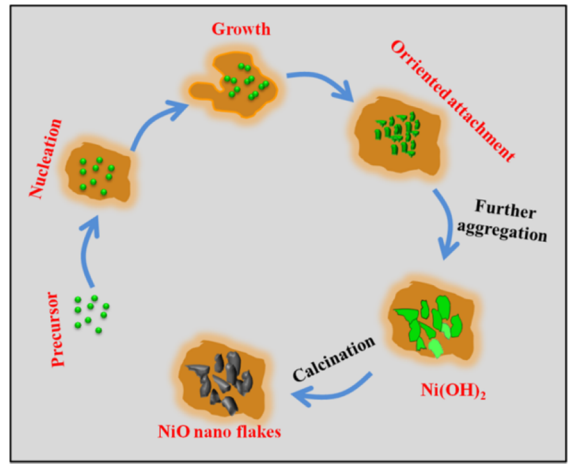

nanoflakes. The formation mechanism of the NiO nanoflakes includes the following: nucleation, growth, and oriented attachment.[28] The nucleation is strongly dependent on the degree of supersaturation. In the nucleation stage, the supersaturation is very high and electrostatic repulsive barriers

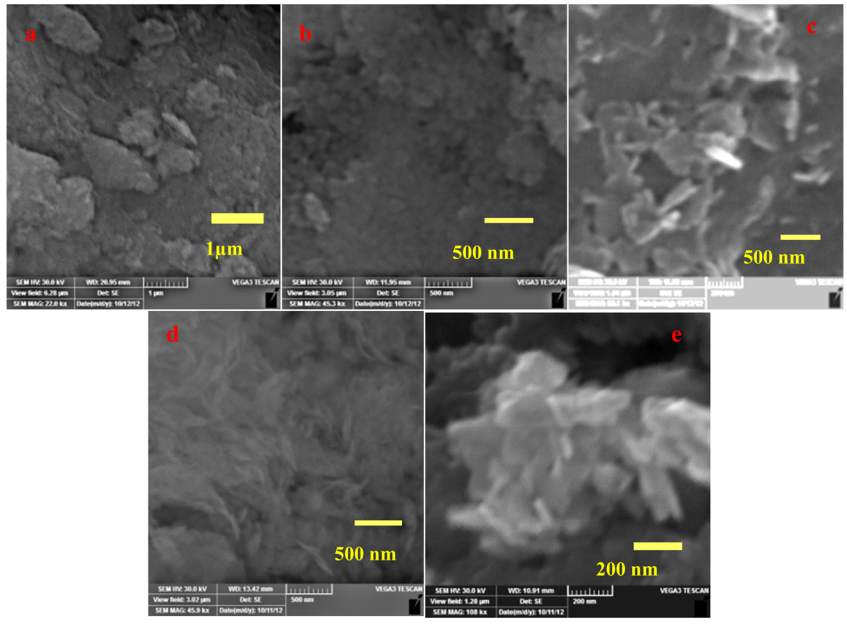

Figure 5. SEM images of particles prepared from the precursor (before any calcination), after exposure to microwaves for (a) 1, (b) 2, (c) 3, (d) 4, and (e) 5 min.

dx.doi.org/10.1021/am400012h | ACS Appl. Mater. Interfaces 2013, 5, 2188−2196

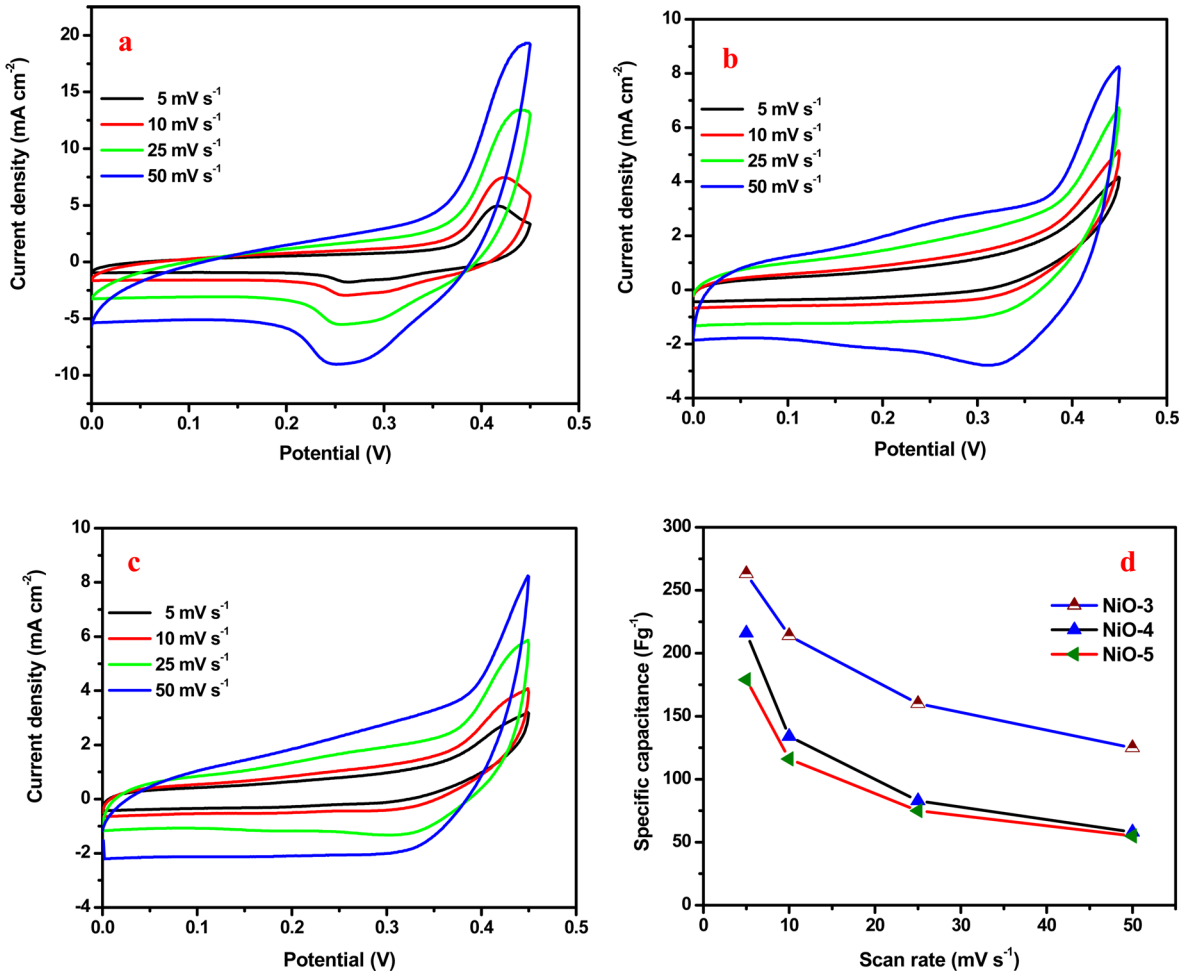

Figure 6. CV curves of (a) NiO-3, (b) NiO-4, and (c) NiO-5 and (d) variation of specific capacitance with scan rate for the three cases.

are low, hence particles tend to aggregate. Microwave accelerates the nucleation rate and also enhances the growth process. The adjoining nanoparticles grow along particular crystal orientation due to the oriented attachment and form nanoflakes. Xu et al.[18] have attributed the formation of $Ni(OH)_2$ flakes under microwave irradiation heating to aggregation of nanocrystals. Further aggregation leads to the thicker $Ni(OH)_2$ nanoflakes. Finally, the flakelike $Ni(OH)_2$ converted into NiO nanoflakes by calcination. During synthesis, CTAB play a crucial role in preventing the random aggregation of nanocrystals and helps to develop the specific morphology. To understand the role of CTAB, the $Ni(OH)_2$ has been synthesized without CTAB and the morphology has been studied using SEM. Figure S1 in the Supporting Information shows the SEM image of $Ni(OH)_2$ synthesized without CTAB. The $Ni(OH)_2$ synthesized without CTAB gives poor morphology. Zheng et al.[17] also investigated the role of CTAB in the development of specific morphology in the synthesis of nickel oxide. Meher et al.[24] also reported the nickel oxide nanomaterial synthesized using CTAB to be of specific morphology whereas nickel oxide synthesized without CTAB yields no specific morphology.

3.3. Electrochemical Studies. The structure and morphology of the electrode material greatly influence on the electrochemical performance.[29] Nanoparticles provide lager surface for a specific volume. This enables better intercalation of charges into the material. The calcination temperature affects the morphology of the material and electrochemical properties.[30] Hence, NiO-3, NiO-4, and NiO-5 electrodes have been employed to cyclic voltammetric, charge−discharge, and impedance test to study the influence of calcination temperature on the electrochemical properties of NiO and to identify the optimum temperature for calcination.

Cyclic voltammetry studies have been performed on NiO-3, NiO-4, and NiO-5 electrodes in a potential window of 0−0.45 V using 2.0 M KOH as an electrolyte. Generally, a NiO electrode in alkaline electrolyte store charges at the electrode/electrolyte interface (electric double layer) and electrode surface (through redox reactions).[13] Figure 6a−c displays the CV curve of NiO-3, NiO-4, and NiO-5 electrodes for different scan rates. CV curves exhibit well-defined redox peaks confirming the Faradic nature of the NiO rather than EDLC which is an ideal rectangular shape. The oxidation and reduction peaks of their respective anodic and cathodic scan are not symmetric. This is due to kinetic irreversibility of the redox process.[31] The charge storage of NiO electrodes arises from the following redox reaction,[31]

$$NiO + zOH^- \Leftrightarrow zNiOOH + (1 - z)NiO + ze^- \quad (1)$$

From the CV curves, it can be noted that the NiO-3 electrode exhibits maximum area under the curve, than NiO-4 and NiO-5 electrodes. Hence, NiO-3 is identified to possess better electrochemical property. The results of CV curve were

dx.doi.org/10.1021/am400012h | ACS Appl. Mater. Interfaces 2013, 5, 2188−2196

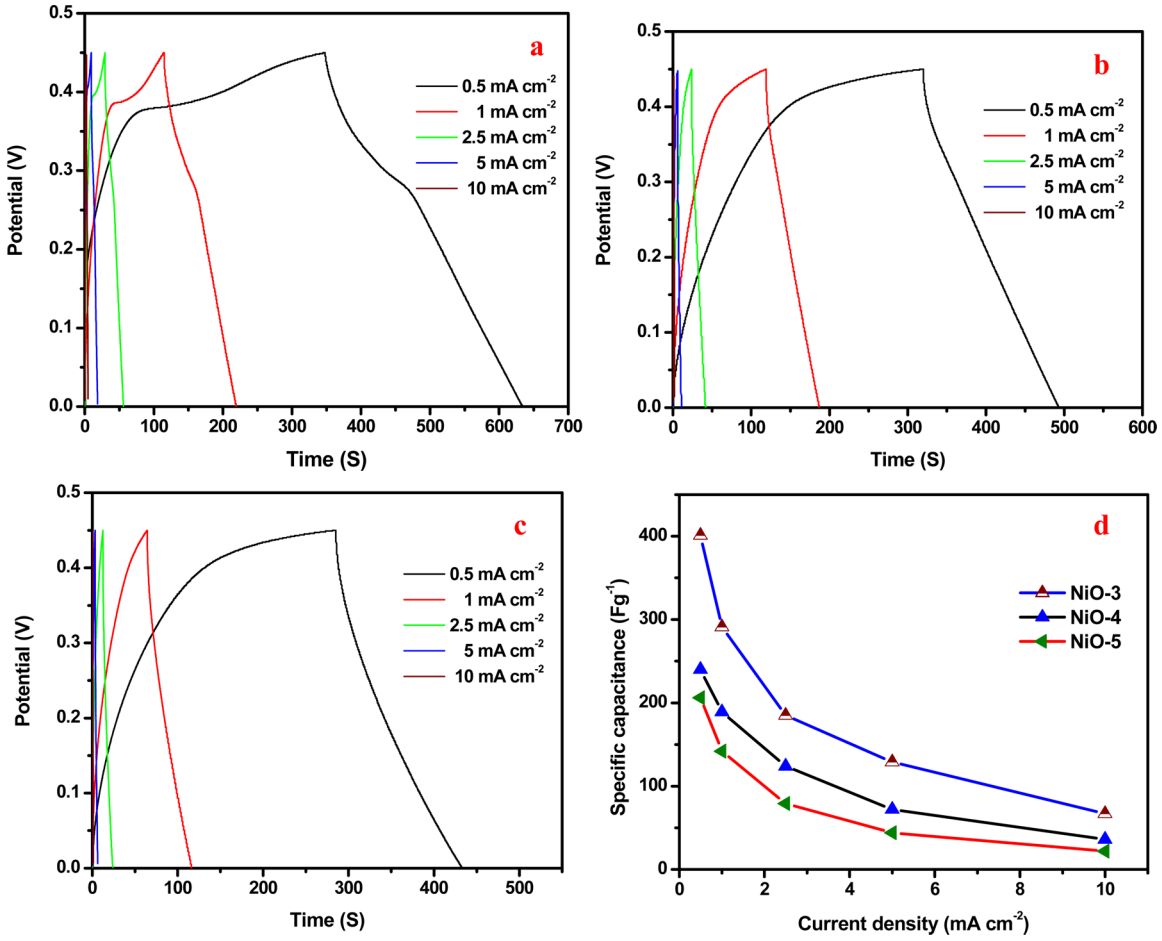

Figure 7. Charge−discharge curves of (a) NiO-3, (b) NiO-4, and (c) NiO-5 and (d) variation of specific capacitance with current density for the three cases.

quantified by calculating the specific capacitance (C_s, F g^{-1}) values using the formula,[32]

$$C_s = \frac{Q}{m\Delta V} \tag{2}$$

Where, Q (C) is the average charge during anodic and cathodic scan, m (g) is the mass of the active material, and ΔV (V) is the applied voltage window. The estimated specific capacitance values are 263, 216, and 179 F g^{-1} for NiO-3, NiO-4, and NiO-5 electrodes at a scan rate of 5 mV s^{-1}. Figure 6d shows the specific capacitance vs scan rate curve for NiO-3, NiO-4, and NiO-5 electrodes. The CV curves were run at different scan rates to further understand the capacity behavior. From the specific capacitance vs scan rate curve, it is observed that the specific capacitance decreases while increasing scan rate. This decrease of specific capacitance can be explained by the ion-exchange mechanism.[33] At low scan rate the OH^- ions have enough time to diffuse into the NiO electrode whereas at high scan rate the diffusion of ions is not aided as the ion have less time to intercalate into the electrode. This lower degree of accessibility for ions to the electrode decreases the specific capacitance value. In all the three NiO electrodes, NiO-3 exhibits maximum specific capacitance at all scan rates. The nanoflakelike morphology of NiO-3 appears to offer higher degree of diffusion of ions in the electrolyte to the NiO electrode and thus result in higher specific capacitance.[34]

The cyclic behavior, stability, and slow-charge and fast-discharge test have been carried out using the chronopotentiometry technique. The charge−discharge measurement was carried out at different current densities from 0 to 0.45 V using 2.0 M KOH as the electrolyte. Figure 7a−c shows the charge−discharge curve of NiO-3, NiO-4, and NiO-5 electrodes. All the nonlinear charge−discharge curves confirm the pseudocapacitance nature of the NiO electrodes, which is in agreement with the CV results.[35] A sloped variation of the charge−discharge curve from ∼0.3 to 0.45 V confirms the pseudocapacitance nature due to redox reaction at the electrode/electrolyte interface, but a small linear variation of the charge−discharge curve from 0 to ∼0.3 V indicates the double-layer capacitance behavior due to the charge separation between the electrode/electrolyte interfaces. The specific capacitance, C_s (F g^{-1}), values were calculated using the formula[32,36]

$$C_s = \frac{i\Delta t}{m\Delta V} \tag{3}$$

Where i (A) is discharge current, m (g) is the mass of the active material, ΔV (V) is the potential window during the discharge, and Δt (s) is the discharge time. The specific capacitance values obtained from charge−discharge studies are 401, 240, and 206 F g^{-1} for NiO-3, NiO-4, and NiO-5 electrodes at a current density of 0.5 mA cm^{-2}. This higher specific capacitance of NiO-3 electrode is due to the nanoflakes like structure of NiO. The nanoflakes like structure act as an "ion-buffering reservoirs"

dx.doi.org/10.1021/am400012h | ACS Appl. Mater. Interfaces 2013, 5, 2188−2196

that reduce the diffusion lengths for the electrolyte ions and enhances the Faradic redox process for charge storage. The specific capacitance of our material (NiO nanoflakes) is higher than NiO nanoflakes synthesized by hydrothermal method. Justin et al.[37] reported the synthesis of porous NiO nanoflakelike morphology via hydrothermal method, showing specific capacitance of 282 F g^{-1} at 0.5 A g^{-1}. Similarly, Zheng et al.[17] reported the specific capacitance of 131.6 F g^{-1} at 0.5 A g^{-1} for NiO nanoflakes synthesized via hydrothermal method. Figure 7d shows the specific capacitance vs current density curve for NiO-3, NiO-4, and NiO-5. The specific capacitance value decreases while increasing current density.[38] The voltage drop in the discharge curve increases while increasing the current density and decrease the specific capacitance value.[39] At low current density, the OH^- ions have enough time to transfer between the electrolyte and the surface of the NiO than at a high current density, resulting higher specific capacitance.

The OH^- ion access by the NiO nanoflake surfaces has been presented in Scheme 2. The flakelike structure composed of nanoparticles reduces the ion diffusion paths and provides more paths for electron conduction.

Scheme 2. Schematic Representation of Accessibility of Ions into the NiO Nanoflake Electrode

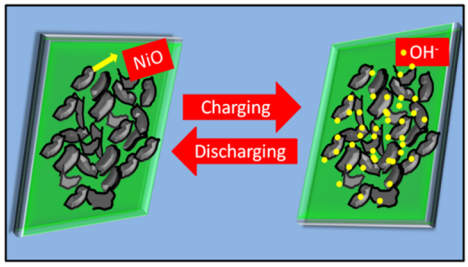

The electrochemical utilization of NiO electrode can be calculated from the following equation[40]

$$z = C\Delta V\frac{M}{F} \quad (4)$$

Where C is the specific capacitance value (F g^{-1}) at 0.5 mA cm^{-2}, ΔV is the potential window, M is the molecular weight of NiO (74.692 g), and F is the Faradic constant. The z value is 1 if the entire electroactive material is involved in the redox process. The calculated "z" values of NiO-3, NiO-4, and NiO-5 are 0.1396, 0.0835, and 0.0717. From this it could be observed that about 14% of sites are involved in the flakes treated at 300 °C which in the other two only 8.4% and 7.2% of the sites are involved. The material prepared at 300 °C, where 14% of the electroactive sites are involved in the redox process gives the maximum specific capacitance of 401 F g^{-1}.

Though supercapacitors can release stored charges quickly at high discharge rates, considering the fact that the energy generation in wind mills and photovoltaic panels is at a slower rate compared to power delivery rates, slow-charge and fast-discharge tests have been carried out on the prepared materials.[41] The results are presented in Figure 8. The NiO-3 electrode was first charged at 0.5 mA cm^{-2}, and continuously discharged at higher current density. The specific capacitance calculated from the discharge portion of slow-charge and fast-discharge test are 246 (2.5), 199 (5), and 144 (10 mA cm^{-2}) F g^{-1}. These values are higher than the values calculated from constant charge−discharge. The cyclic stability of the electrode

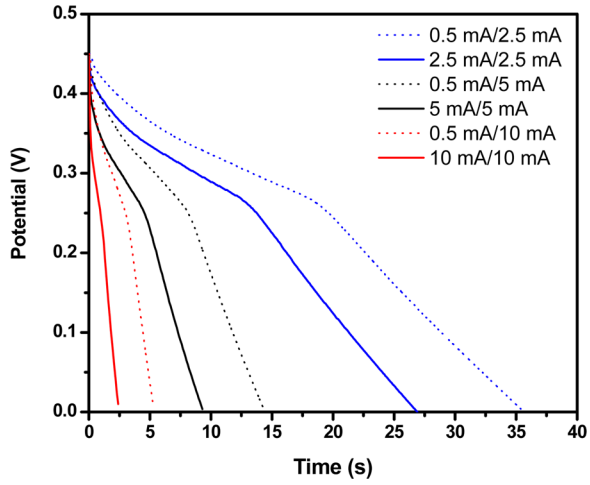

Figure 8. Slow-charge and fast-discharge curve of NiO-3.

material is very important for practical supercapacitor applications. The nickel oxide nanoflake (NiO-3) electrode was employed in charge−discharge test at 10 mA cm^{-2} up to 500 cycles. Figure 9 shows the profile of capacitance retention

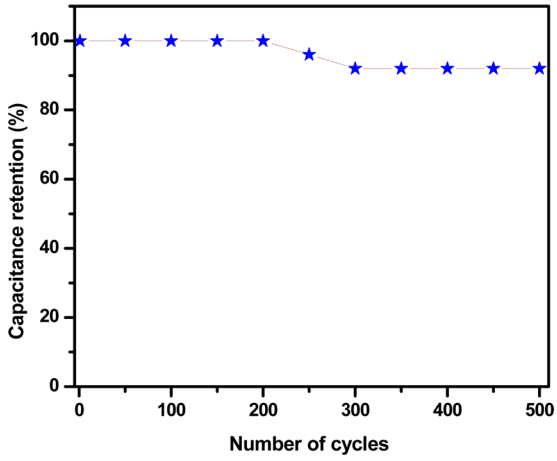

Figure 9. Capacitance retention with cycles of charge−discharge of NiO-3.

with number of cycles. Even after, 500 continuous charge−discharge cycles the NiO nanoflakes retain 92% of the initial capacitance. This higher capacitance retention implies that the NiO nanoflakes are suitable material for supercapacitor application.

Figure 10a shows the impedance plot of NiO-3, NiO-4, and NiO-5 electrodes in the frequency range of 0.01−100 kHz at a bias potential of 0.4 V. The inset of Figure 10a show the high frequency region of the impedance plot and fitting circuit. In the fitting circuit, R_s and R_{ct} are solution and charge-transfer resistance, respectively. C_{dl} is the double layer capacitance, C_p is the pseudocapacitance, and "W" is the Warburg impedance. The intercept at high frequency on the real axis is solution resistance (R_s). The R_s values of NiO-3, NiO-4, and NiO-5 electrodes are 1.35, 1.38, and 1.56 Ω, respectively. This solution resistance is the combination of (i) ionic and electronic resistances, (ii) intrinsic resistance of the NiO electrodes, and (iii) diffusive as well as contact resistance at the NiO electrode/current collector interface.[42] The semicircle at high frequency

dx.doi.org/10.1021/am400012h | ACS Appl. Mater. Interfaces 2013, 5, 2188−2196

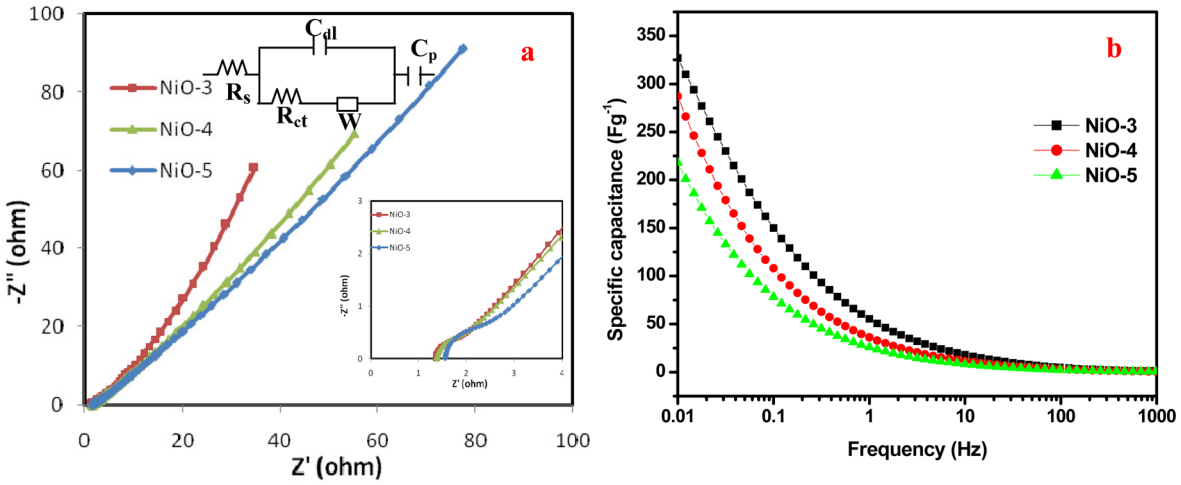

Figure 10. (a) Impedance plot of NiO electrodes at 0.4 V, (inset) equivalent fitting circuit and impedance at high frequency region, and (b) frequency dependent specific capacitance of NiO electrodes.

region belongs to the charge transfer resistance (R_{ct}) of the electrode.

This R_{ct} is related to the electroactive surface area of the electrode, due to the Faradic redox process of the NiO electrodes involving in the exchange of OH^- ions.[42] R_{ct} values of NiO-3, NiO-4, and NiO-5 electrodes are 0.40, 0.46, and 0.72 Ω, respectively. The flakelike morphology of NiO-3 could enhance the diffusivity of the electrolyte in the electrode results, lowering the charge-transfer resistance value.[43] The straight line portion at low frequency region corresponds to Warburg impedance, *W*, of the NiO electrodes during redox process. The lower slope of NiO-3 electrode indicates the faster ion diffusion of electrolyte than NiO-4 and NiO-5. The specific capacitance values of the NiO electrodes were calculated from the impedance measurements using the relation[24,44]

$$C_s = \frac{1}{2\pi f Z''} \quad (5)$$

Figure 10b shows the frequency dependent specific capacitance curve of NiO electrodes at bias potential of 0.4 V. The specific capacitance values of NiO-3, NiO-4, and NiO-5 electrodes are 327, 287, and 218 F g^{-1}. This result is in good agreement with the cyclic voltammetric and charge−discharge results.

4. CONCLUSION

The nickel oxide nanoflakes are synthesized successfully using microwave heating method. The XRD analysis reveals the synthesized NiO are cubic phase. SEM images of NiO calcined at 300 °C show nanoflakes structure. Time evaluation study suggests 5 min of microwave heating develops the nanoflakelike structure. CTAB plays a crucial role in preventing the random agglomeration of nanocrystals. The NiO nanoflakes exhibit maximum specific capacitance of 401 F g^{-1} at 0.5 mA cm^{-2}. The nanoflakelike structure acts as an "ion-buffering reservoir" that reduces the diffusion lengths for the electrolyte ions. The charge-transfer resistance value of NiO-3 electrode is 0.40 Ω. Hence, NiO nanoflakes are a suitable electrode material for supercapacitor applications.

■ ASSOCIATED CONTENT

Ⓢ Supporting Information

SEM image of $Ni(OH)_2$ synthesized without CTAB. This material is available free of charge via the Internet at http://pubs.acs.org.

■ AUTHOR INFORMATION

Corresponding Author

*E-mail: muraligru@gmail.com. Tel.: +91 451 2452371. Fax: +91 451 2454466.

Notes

The authors declare no competing financial interest.

■ REFERENCES

(1) Simon, P.; Gogotsi, Y. *Nat. Mater.* **2008**, *7*, 845−854.
(2) Hall, P. J.; Mirzaeian, M.; Fletcher, S. I.; Sillars, F. B.; Rennie, A. J. R.; Shitta-bey, G. O.; Wilson, G.; Cruden, A.; Carter, R. *Energy Environ. Sci.* **2010**, *3*, 1238−1251.
(3) Liu, C.; Yu, Z.; Neff, D.; Zhamu, A.; Jang, B. Z. *Nano Lett.* **2010**, *10*, 4863−4868.
(4) Shukla, A. K.; Sampath, S.; Vijayamohan, K. *Curr. Sci.* **2000**, *79*, 1656−1661.
(5) Hu, C. C.; Chang, K. H.; Lin, M. C.; Wu, Y. T. *Nano Lett.* **2006**, *6*, 2690−2695.
(6) Zhu, J.; He, J. *ACS Appl. Mater. Interfaces* **2012**, *4*, 1770−1776.
(7) Xia, X. H.; Tu, J. P.; Wang, X. L.; Gu, C. D.; Zhao, X. B. *J. Mater. Chem.* **2011**, *21*, 671−679.
(8) Cheng, H.; Lu, Z. G.; Deng, J. Q.; Chung, C. Y.; Zhang, K.; Li, Y. Y. *Nano Res.* **2010**, *3*, 895−901.
(9) Brezesinski, T.; Wang, J.; Tolbert, S. H.; Dunn, B. *Nature mater* **2010**, *9*, 146−151.
(10) Dong, S.; Chen, X.; Gu, L.; Zhou, X.; Xu, H.; Wang, H.; Liu, Z.; Han, P.; Yao, J.; Wang, L.; Cui, G.; Chen, L. *ACS Appl. Mater. Interfaces* **2010**, *3*, 93−98.
(11) Deng, W.; Liu, Y.; Zhang, Y.; Lu, F.; Chen, Q.; Ji, X. *RSC Advances* **2012**, *2*, 1743−1745.
(12) Lang, J. W.; Kong, L. B.; Wu, W. J.; Luo, Y. C.; Kang, L. *Chem. Commun.* **2008**, 4213−4215.
(13) Yuan, C.; Zhang, X.; Su, L.; Gao, B.; Shen, L. *J. Mater. Chem.* **2009**, *19*, 5772−5777.
(14) Xiong, S.; Yuan, C.; Zhang, X.; Qian, Y. *CrystEngComm* **2011**, *13*, 626−632.
(15) Ding, S.; Zhu, T.; Chen, J. S.; Wang, Z.; Yuan, C.; (David) Lou, X. W. *J. Mater. Chem.* **2011**, *21*, 6602−6606.
(16) Wu, M. S.; Wang, M. J. *Chem. Commun.* **2010**, *46*, 6968−6970.

(17) Zheng, Y. Z.; Ding, H. Y.; Zhang, M. L. *Mater. Res. Bull.* **2009**, *44*, 403−407.
(18) Xu, L.; Ding, Y. S.; Chen, C. H.; Zhao, L.; Rimkus, C.; Joesten, R.; Suib, S. L. *Chem. Mater.* **2008**, *20*, 308−316.
(19) Jhung, S. H.; Jin, T.; Hwang, Y. K.; Chang, J. S. *Chem.—Eur. J.* **2007**, *13*, 4410−4417.
(20) Bilecka, I.; Niederberger, M. *Nanoscale* **2010**, *2*, 1358−1374.
(21) Obermayer, D.; Gutmann, B.; Kappe, C. O. *Angew. Chem., Int. Ed.* **2009**, *48*, 8321−8324.
(22) Ren, Y.; Gao, L. *J. Am. Ceram. Soc.* **2010**, *93*, 3560−3564.
(23) Cao, C. Y.; Guo, W.; Cui, Z. M.; Song, W. G.; Cai, W. *J. Mater. Chem.* **2011**, *21*, 3204−3209.
(24) Meher, S. K.; Rao, G. R. *ACS Appl. Mater. Interfaces* **2011**, *3*, 2063−2073.
(25) Li, J.; Zhao, W.; Huang, F.; Manivannan, A.; Wu, N. *Nanoscale* **2011**, *3*, 5103−5109.
(26) Hajry, A. A.; Umar, A.; Vaseem, M.; Assiri, M. S. A.; Tantawy, F. E.; Bououdina, M.; Heniti, S. A.; Hahn, Y. B. *Superlattice Microst.* **2008**, *44*, 216−222.
(27) Lee, J. W.; Ahn, T.; Kim, J. H.; Ko, J. M.; Kim, J. D. *Electrochim. Acta* **2011**, *56*, 4849−4857.
(28) Ran, S.; Zhu, Y.; Huang, H.; Liang, B.; Xu, J.; Liu, B.; Zhang, J.; Xie, Z.; Wang, Z.; Ye, J.; Chen, D.; Shen, G. *CrystEngComm* **2012**, *14*, 3063−3068.
(29) Zhang, X.; Shi, W.; Zhu, J.; Zhao, W.; Ma, J.; Mhaisalkar, S.; Maria, T. L.; Yang, Y.; Zhang, H.; Hng, H. H.; Yan, Q. *Nano Res* **2010**, *3*, 643−652.
(30) Sun, X.; Wang, G.; Hwang, J. Y.; Lian, J. *J. Mater. Chem.* **2011**, *21*, 16581−16581.
(31) Meher, S. K.; Justin, P.; Rao, G. R. *Nanoscale* **2011**, *3*, 683−692.
(32) Yan, J.; Khoo, E.; Sumboja, A.; Lee, P. S. *ACS Nano* **2010**, *4*, 4247−4255.
(33) Pang, H.; Zhang, B.; Du, J.; Chen, J.; Zhang, J.; Li, S. *RSC Adv.* **2012**, *2*, 2257−2261.
(34) Jiang, H.; Zhao, T.; Li, C.; Ma, J. *J. Mater. Chem.* **2011**, *21*, 3818−3823.
(35) Jiang, H.; Sun, T.; Li, C.; Ma, J. *RSC Adv.* **2011**, *1*, 954−957.
(36) Wang, N.; Wu, C.; Li, J.; Dong, G.; Guan, L. *ACS Appl. Mater. Interfaces* **2011**, *3*, 4185−4189.
(37) Justin, P.; Meher, S. K.; Rao, G. R. *J. Phys. Chem. C* **2010**, *114*, 5203−5210.
(38) Gao, H.; Xiao, F.; Ching, C. B.; Duan, H. *ACS Appl. Mater. Interfaces* **2012**, *4*, 7020−7026.
(39) Liu, M.-C.; Kong, L.-B.; Lu, C.; Li, X.-M.; Luo, Y.-C.; Kang, L. *ACS Appl. Mater. Interfaces* **2012**, *4*, 4631−4636.
(40) Srinivasan, V.; Weidner, J. W. *J. Electrochem. Soc.* **2000**, *147*, 880−885.
(41) Lu, Q.; Lattanzi, M. W.; Chen, Y.; Kou, X.; Li, W.; Fan, X.; Unruh, K. M.; Chen, J. G.; Xiao, J. Q. *Angew. Chem., Int. Ed.* **2011**, *123*, 6979−6982.
(42) Wu, M. S.; Hsieh, H. H. *Electrochim. Acta* **2008**, *53*, 3427−3435.
(43) Zhang, J.; Kong, L. B.; Cai, J. J.; Li, H.; Luo, Y. C.; Kang, L. *Micropor. Mesopor. Mat.* **2010**, *132*, 154−162.
(44) Conway, B. E. *Electrochemical Supercapacitors: Scientific Fundamentals and Technological applications*; Kluwer Academic/Plenum: New York, 1999.